J Mater Sci (2010) 45:3683–3696
DOI 10.1007/s10853-010-4541-1

REVIEW

# Crystallization in glass: elucidating a realm of diversity by transmission electron microscopy

**Thomas Höche**

Received: 17 March 2010 / Accepted: 19 April 2010 / Published online: 6 May 2010


**Abstract** Glass ceramics, i.e. intentionally devitrified glasses, are used in manifold applications. This is due to the capability to precisely control the precipitation of crystalline phases possessing useful properties related to optics, mechanics, biocompatibility, piezoelectricity, machinability, etc. In order to control the nano and microstructure, transmission electron microscope imaging proves particularly useful. Illustrated by numerous examples, the diverse precipitate shapes and mechanisms at work upon crystallization of glasses are discussed. In addition, it is shown how useful cutting-edge transmission electron microscopy is in the field of nanoanalytics. The investigation of nanoscale processes controlling the precipitation of functional crystals evidences the need for more sophisticated theories describing the changes of composition accompanying crystallization in non-isochemical systems (precipitates possess compositions different from those of the host glasses).

## Introduction

Glasses do exist on earth for ages, for example as obsidian, a volcanic glass that is formed upon cooling of lava under suitable conditions. The latter natural glass has already been used by Stone Age cultures as it can be fractured to produce blades or arrowheads. Glass could, however, only in the Bronze Age become manufactured artificially. Glass-making technology is believed have its roots in Egypt and Western Asia.

T. Höche (✉)
Leibniz-Institut für Oberflächenmodifizierung e.V,
Permoserstraße 15, 04318 Leipzig, Germany
e-mail: thomas.hoeche@iom-leipzig.de

Similar to obsidian, where the inclusion of white cristobalite crystals in the deep black glass can produce a very conspicuous snowflake pattern, devitrification, i.e. the precipitation of crystals from the glass upon making, turned out to be a major issue in man-made glasses. This is because glasses that do contain not too small crystals (see below) are no longer transparent. Over the years, however, a rich knowledge about means to suppress devitrification has been gained, including the proper choice of glass composition and technologies to increase cooling rates. Moreover, it became evident that glass formation can only be attained for a limited range of compositions.

While in the beginning of glass making, flawless, fully transparent glasses were aimed at, later on, sophisticated glasses with tailored physical and chemical properties were "/>focussed at. In the medieval age, colouring of glass to be used in church windows became widely used, without realizing the origin of colour. Besides adding fairly high amounts of transition metals such as $Cu^{2+}$, $Co^{2+}$ or $Mn^{3+}$, all resulting in "direct" colouring, in ruby glasses, surface plasmons provoked at metal nanoparticles are responsible for the optical effect of colouring.

Based on a broad empirical knowledge on how glasses with suitable optical properties can be made, it was only by the middle of last century that scientific studies to classify and understand the microstructure of glasses were launched. The whole variety of liquid–liquid phase separations in glass became apparent by that time, including for example droplets in a residual-glass matrix, intercalation structures, as well as secondary, ternary, etc. phase-separation phenomena [1].

At this point, electron microscopy came forward. Besides scanning electron microscopy, capable of imaging the surface topography of fractured and/or superficially etched glasses, transmission electron microscopy turned

out to provide valuable information on the microstructure at very high spatial resolution. The beauty of this method is that real images can be obtained and size, size distribution etc. are directly accessible and not just the result of fitting models to "anonymous" spectra. Of course, as always, the broadest picture can be drawn when as much methods as possible are combined to study one and the same material.

As in these early days, electron-transparent sections could be hardly prepared (the way to do it was crushing glass into fine pieces), the replica technique was elaborated [2]. In the latter approach, a freshly fractured or etched surface of a glass is coated by co-evaporation of carbon and a mixture of Pt and Pd under an oblique angle. The basic idea is that highly mobile carbon would migrate towards shadowed parts of the topography, while the metals decorate the topography much more locally, resulting in different thicknesses of the Pt/Pd alloy dependent on the laterally varying inclination of the specimen's topography. The film, continuously expanding over the surface due to surface diffusion of carbon, is detached in water and fetched with a TEM grid for inspection. As an example, in Fig. 1, the phase-separation structure of a soldering glass used for ignition plugs is shown.

Upon preparation, information of the replica film's relative orientation towards the source of deposition gets lost. Therefore, $MoO_2$ crystals can be deposited onto the surface prior to synthesis of the replica film. As the $MoO_2$ crystals always protrude from the surface, discrimination between elevated and recessed structures is doubtlessly possible. Imaging of replica films is, however, an essentially indirect technique as the topographic impression gained is neither quantitative (in the sense that the height or depth of structures can be measured) nor can the chemical nature of adjacent areas be directly assessed. The latter can only be estimated for etched surfaces based on prior knowledge (like: HCl preferably attacks Si-rich parts of the microstructure, hence recessed structures are likely to contain more Si than its surroundings). Moreover, the spatial resolution is limited by the inherent structure of the film as shown in Fig. 2. As a rule of thumb, a spatial resolution of better than 3–5 nm cannot be reached (for this reason).

In spite of the great importance, replica films historically had for the development of an understanding of glass microstructures, the lack of direct chemical sensitivity and resolution brought about the need for alternative preparation routes. In this respect, the development of ion-beam etching as well as ultramicrotomy for TEM sample preparation [3] turned out to become a very valuable tool as with these approaches much higher spatial resolution can be realized as well as chemical information on the nanoscale can be obtained. While ion-beam thinning is widely accepted for TEM preparation, ultramicrotomy is still a niche technology in which a precisely edged diamond knife is used to cut electron-transparent sections. This is most likely due to the fact that it requires a very skilful person to conduct the cutting and experiences need to be gained for every unknown materials system, while ion-beam etching is relatively rugged approach.

In this review, the value of various TEM techniques for studying not just the structure of glasses but also time- and temperature-dependent crystallization of glasses will be vaunted. Before entering into the details, however, a few

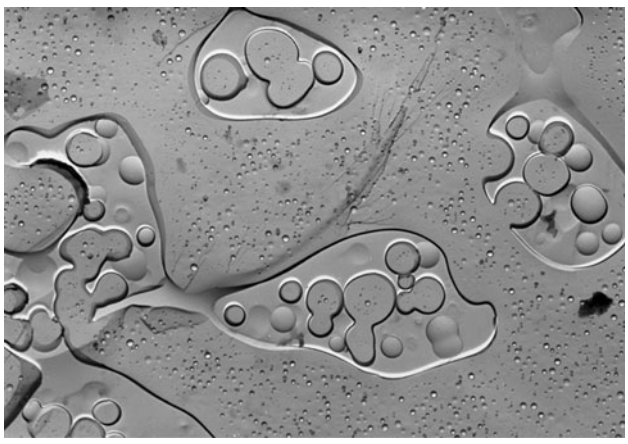

**Fig. 1** TEM bright-field micrograph of a replica film obtained from the polished surface of an ignition-plug soldering glass etched with a 1:1 mixture of 2.5% HF and 2.5% $HNO_3$ for 5 s (followed by cleaning in distilled water followed and deposition of a Pt–Ir–C thin film under an angle of 45°)

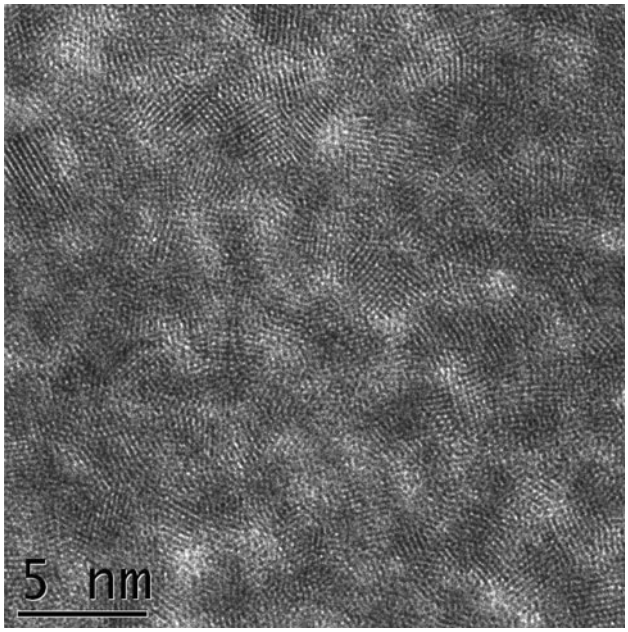


**Fig. 2** HRTEM micrograph of a Pt–Ir–C replica film demonstrating the inherent limitations of spatial resolution: at high resolution, the topographic information gets superimposed by the internal structure of the film and diffraction contrast interferes

introductory words about glass ceramics, i.e. partly crystallized glasses made by intention, need to be said.

In order to tailor materials properties or their combinations, it is very reasonable to think about partially crystallizing glasses. First, glasses can be easily casted and shaped into desired shapes and upon subsequent crystallization shrinking is much less severe than during sintering of powders. Second, it is appealing to host functional properties in tiny crystals that are embedded in a transparent, less brittle matrix. For example, single crystals of fresnoite, $Ba_2TiSi_2O_8^5$ and $Ba_2TiGe_2O_8$ [4], possess very pronounced piezoelectric and pyroelectric properties, making them ideal candidates for hydrophone applications. However, although single crystals can be grown by the Czochralski technique, the latter are so sensitive towards mechanical strain that the only way to use these materials is to precipitate grain-oriented fresnoite crystals in a glassy matrix taking up the strain [5–7]. Another example concerns mechanically and chemically resistant alumosilicate glasses containing fluoride crystals that are—due to their low phonon energy—suited best to host rare-earth dopands for lasing, upconversion and other optical applications [8, 9].

The usage of partially crystalline materials for optical applications raises the questions of transparency. As pointed out already in the late 1960s by Beall and Duke [10], there are several factors influencing the transparency of glass ceramics for a given wavelength of the light: the crystallites' size, their distribution in the matrix and the difference in refractive index of crystals and glassy phase. If the crystals are smaller than one-tenth of the wavelength and not too densely dispersed in a glassy matrix, fully transparent glass ceramics with very interesting optical properties [11–13] can be synthesized.

Independent on whether or not a glass ceramics material is transparent, tailoring properties generally requires a precisely controlled microstructure, which can be imaged best, due to the inherent spatial resolution, by transmission electron microscopy. In particular, the monitoring of changes to the microstructure in dependence of heat-treatment time and temperature, additives, cooling rates, etc. is readily assessable in terms of geometric figures like average size, size distribution, shapes, etc. The necessity to image the microstructure is illustrated by Fig. 3, in which the microstructure of a $PbF_3$-containing glass ceramics is depicted. According to X-ray diffraction, the average size of the crystalline precipitates amounts to roughly 30 nm and only by direct imaging it became evident that dendritic growth takes place resulting in much larger crystalline agglomerates explaining in turn the opaque appearance of this glass ceramics.

Local chemistry, another important aspect of microstructural characterization, can be probed either by energy-dispersive X-ray spectrometry (EDXS) or by electron energy-loss spectroscopy (EELS). Due to a much smaller solid angle of detection, EDXS generally has an inferior sensitivity and is less well-suited for probing elements of atomic number $< 13$ (sodium). Absorption effects and competing Auger electron emission do reduce the detectable X-ray yield for those light elements by EDXS. The latter elements, however, are the domain of EELS. Moreover, energy-filtered TEM imaging, combining structural and chemical information on the nanoscale can be applied.

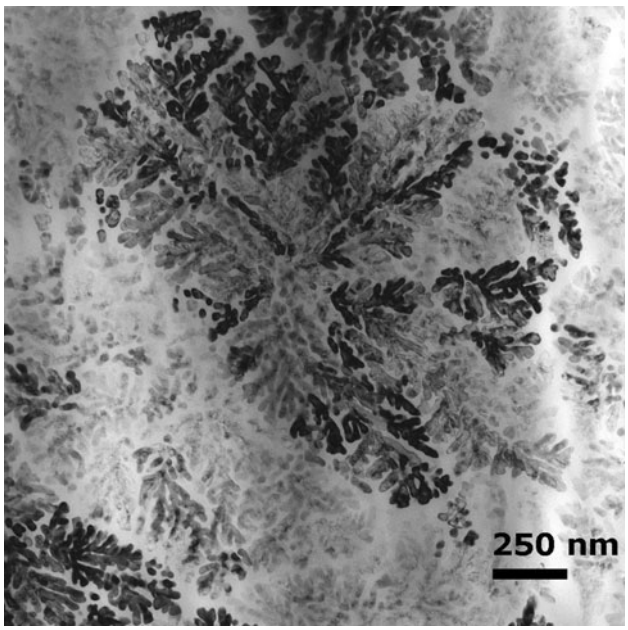


**Fig. 3** $PbF_3$-containing glass ceramics (TEM bright-field micrograph)

In the following, it will be shown by virtue of several examples how conventional as well as advanced TEM techniques can be utilized to elucidate the manifold phenomena related to nucleation and growth of crystalline phases in glasses. Although by far not all melts are forming glasses upon cooling at experimentally assessable cooling rates, it will become apparent that many in terms of applications important crystalline phases can be precipitates in glasses.

## Machinable mica glass ceramics

The main advantage of mica glass ceramics is their machinability [14–16]. Unlike metals or polymers, plastic deformation is not the key to the understanding of this unusual property of a ceramics material. Rather than this, the unique microstructure comprising mica crystals dispersed in a residual glass matrix is responsible for the ability of drilling, milling, tapping, turning and sawing these peculiar glass ceramics. A crack starting to propagate

in the residual glass will readily find a mica crystal on its way. As mica is a highly anisotropic material in terms of its mechanical properties, cleavage along the sheet plane of the layer-like structure is rather easy, whereas crack propagation perpendicular to it is hardly possible. Therefore, a crack will become deflected to either follow the mica–glass interface or propagate within the mica sheet planes. As cleavage dissipates energy, the energy of the propagating crack is reduced with every deflection and cleavage release until the crack comes to a halt. Bioactive micaceous glass ceramics are applied as dental materials [17], for calva replacements, or ossicle implants [18].

Although mica crystals, due to their layer structure, occur generally plate-like, dependent on the composition of the glass they become precipitated from, also other habits may occur. Annealing of a $3.2Na_2O{\cdot}3.2K_2O{\cdot}17.4MgO{\cdot}16.0Al_2O_3{\cdot}48.7SiO_2{\cdot}11.5F^-$ (all mol.%, used throughout this review) glass can, for example, results in the formation of cabbage-shaped mica aggregates as shown in Fig. 4a [19]. A liquid–liquid phase separation was proven to be responsible for this peculiar behaviour. In order to explain TEM observations like the one depicted in Fig. 4b, a growth mechanism was proposed assuming crystallization to take place along isocompositional lines at or not far from the surface of liquid–liquid phase-separation droplets. Due to high growth rates, diffusion is assumed to have only little impact on crystal growth.

While in a $4.1Na_2O{\cdot}3.1K_2O{\cdot}16.8MgO{\cdot}16.9Al_2O_3{\cdot}42.9SiO_2{\cdot}3.5TiO_2{\cdot}12.7F^-$ (titania was added as a nucleation agent) glass gentle adjustments of the composition lead to the formation of plate-like mica crystals, those plates become micro-yoyo-shaped for a slightly different stoichiometry. For example, from a $2.6Na_2O{\cdot}2.5K_2O{\cdot}14.8MgO{\cdot}11.5Al_2O_3{\cdot}57.3SiO_2{\cdot}10.2F^-{\cdot}1.1Cl-$ glass, mica agglomerates like the ones shown in Fig. 5 are formed [20]. Other than the flanking plates, the central necking, being more or less pronounced depending on the heat-treatment schedule, turned out to be highly defective. This defect structure could be attributed to the preceding precipitation of norbergite, $Mg_3F_2SiO_4$, resulting in a $Mg^{2+}$- and $F^-$-depleted glass. Upon dissolving norbergite at elevated temperatures, defective plates become sandwiched between defect-free phlogopite slabs epitaxially formed on faces of the defective mica crystals. The microstructure of the latter glass ceramics could only be studied in fine details since the mica crystals were oriented by extrusion, resulting in a ring-fibre structure [21, 22].

## Biocompatible apatite glass ceramics

The principal inorganic component of the hard tissue is closely related to hydroxyapatite, $Ca_{10}(PO_4)_6(OH)_2$.

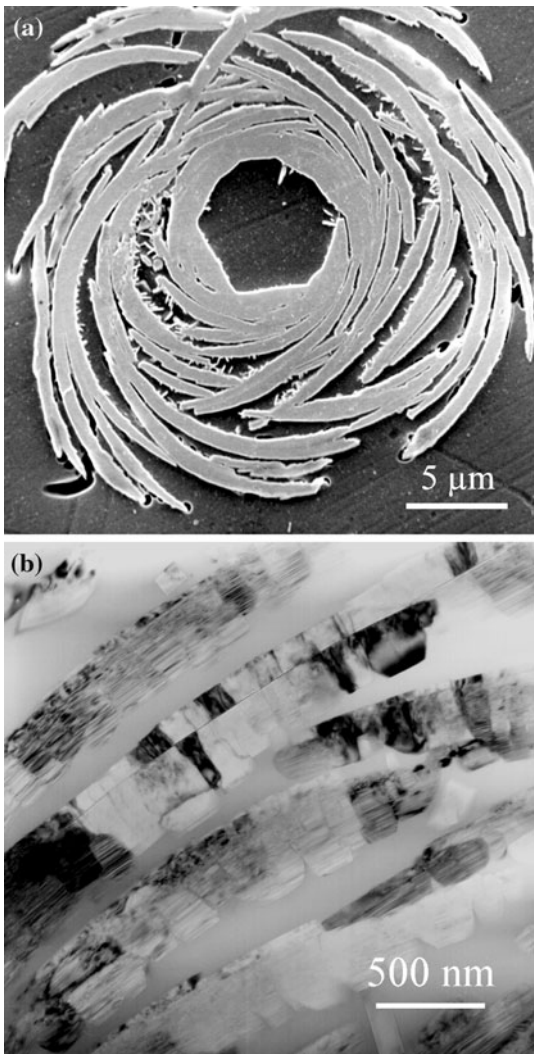


**Fig. 4** **a** SEM micrograph (secondary electron image) of a cabbage-shaped mica crystal aggregate after a gentle superficial etch (reproduced with copyright permission granted by Elsevier [19]). **b** TEM bright-field micrograph of an enlarged section of a cabbage-shaped mica crystal aggregate similar to the one shown in (**a**). Plane mica segments of some 200 nm width are interconnected by small-angle tilt boundaries (reproduced with copyright permission granted by Elsevier [19])

Therefore, it suggests itself to try and precipitate apatite from glasses of suitable composition. Starting with the apatite–wollastonite glass ceramics developed by Kokubo et al. [23], various apatite glass ceramics have been developed and mainly used in restorative dentistry over the past 35 years.

As opposed to mineralized tissue containing oriented elongated apatite crystals, the morphology of apatite crystals in the early glass ceramics used to be isometric and it was only later that glass ceramics containing apatite needles were developed [24–27]. Intense microstructural investigations revealed that the composition (in particular the Ca/P ratio [28]) and heat-treatment schedule [29, 30]

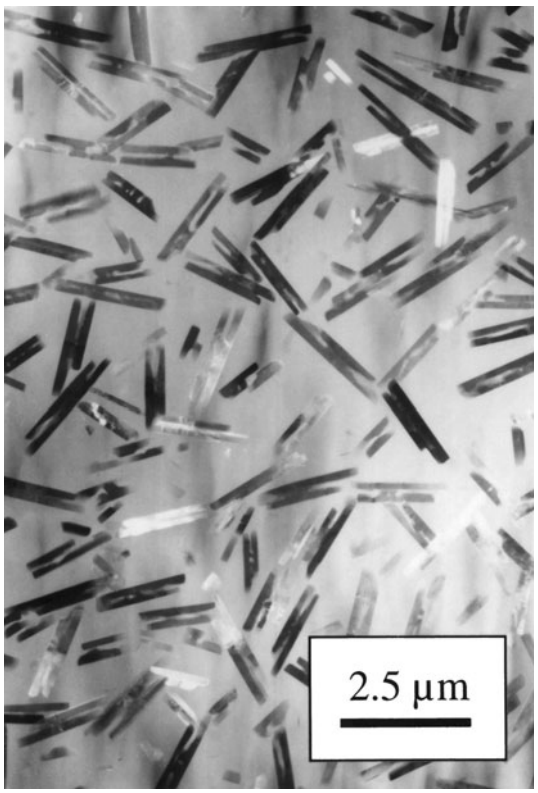


**Fig. 5** TEM bright-field micrograph of yoyo-shaped mica crystals oriented in a ring-fibre texture by extrusion (reproduced with copyright permission granted by Elsevier [20])

sensitively influence the habit of the apatite crystals formed and that also in these glass systems, phase-separation phenomena play a decisive role in the process of crystallization (cf. Fig. 6).

During the study of apatite glass ceramics, a general principle of glass ceramics investigation, namely the combination of spatially resolved and integrating experimental techniques was very successfully applied. Based on data from $^{31}$P MAS NMR spectrometry and imaging as well as energy-dispersive X-ray spectrometry in the transmission electron microscope, phase-separation processes were shown to have a major impact on the composition of the residual glass hosting apatite crystals. The structure and composition of the glass matrix in turn determine the fluorapatite morphology observed. At lower heat-treatment temperatures, spherical crystals become precipitated since growth parallel and perpendicular to the crystallographic *c*-axis of apatite take place with very similar growth rates caused by limited diffusion keeping building units for exaggerate growth short. As the latter restriction gets less influential for higher temperatures, anisometric growth does occur at high temperature. In the latter case, even coarsening of fluorapatite needles following the time-dependence of Ostwald ripening takes place. Thermodynamic considerations indicate that competing growth mechanisms (normal versus spiral growth) along different crystallographic directions are responsible for the strongly direction-dependent growth rates observed at elevated temperatures leading to aspect ratios as large as 15:1 (Fig. 7). From long-term heat treatments, however, it is evident that the needle-shaped morphology is not the equilibrium shape but caused by kinetic growth effects.

## Zero thermal-expansion lithium alumosilicate glass ceramics

One of the top-selling glass ceramics are close-to-zero thermal-expansion materials. The latter glass ceramics are not just used in home appliances like ceramics stove tops & glassy fireplace shields but also employed to fabricate high-tech products such as monolithic telescope-mirror blanks and mask blanks for wafer-stepper lithography. The idea behind such materials is to precipitate nanosized crystals possessing negative thermal expansion at least along one crystallographic direction. Being homogeneously dispersed and non-textured, the volume increase of the base glass (and, if applicable, other crystalline phase) upon heating is compensated by a suitable volume fraction of a phase that shrinks. In order to avoid disintegration of the workpiece, the host glass must be capable of bearing residual local stresses. Such a material given, both high-temperature resistance and thermal-shock resistance can be achieved and shape changes upon heating and cooling become minimized.

One puzzling detail in this respect is the choice of the relatively scarce crystalline phase with negative thermal expansion. Although there are even compounds with isotropic negative coefficients of thermal expansion, like cubic $ZrW_2O_8$ [31] or $ZrV_2O_7$ [32], only a few of them can be precipitated from glass-forming melts. In praxis, $\beta$-eucryptite, $\beta$-spodumen or keatite can crystallize in lithium alumosilicate glasses [33, 34].

Although the latter crystals usually take a fairly high volume fraction, the glass ceramics obtained can be fully transparent [12], due to the sole occurrence of nano-sized crystals. Although such glass ceramics containing nano crystals have been commercialized since decades, the fundamentals of the crystallization process are not yet fully understood [35]. The main question is why in these systems such a high quantity of nanocrystals is formed and crystal growth does not progress even if the material is annealed for very long times, e.g. even for some weeks as in the case of Zerodure$^{TM}$ telescope mirrors [36]. In most other glass ceramics as well as in sintered ceramics, Ostwald ripening would take place if a certain concentration of a crystalline phase is exceeded and nano crystallinity can only be achieved at much smaller volume concentrations. It was

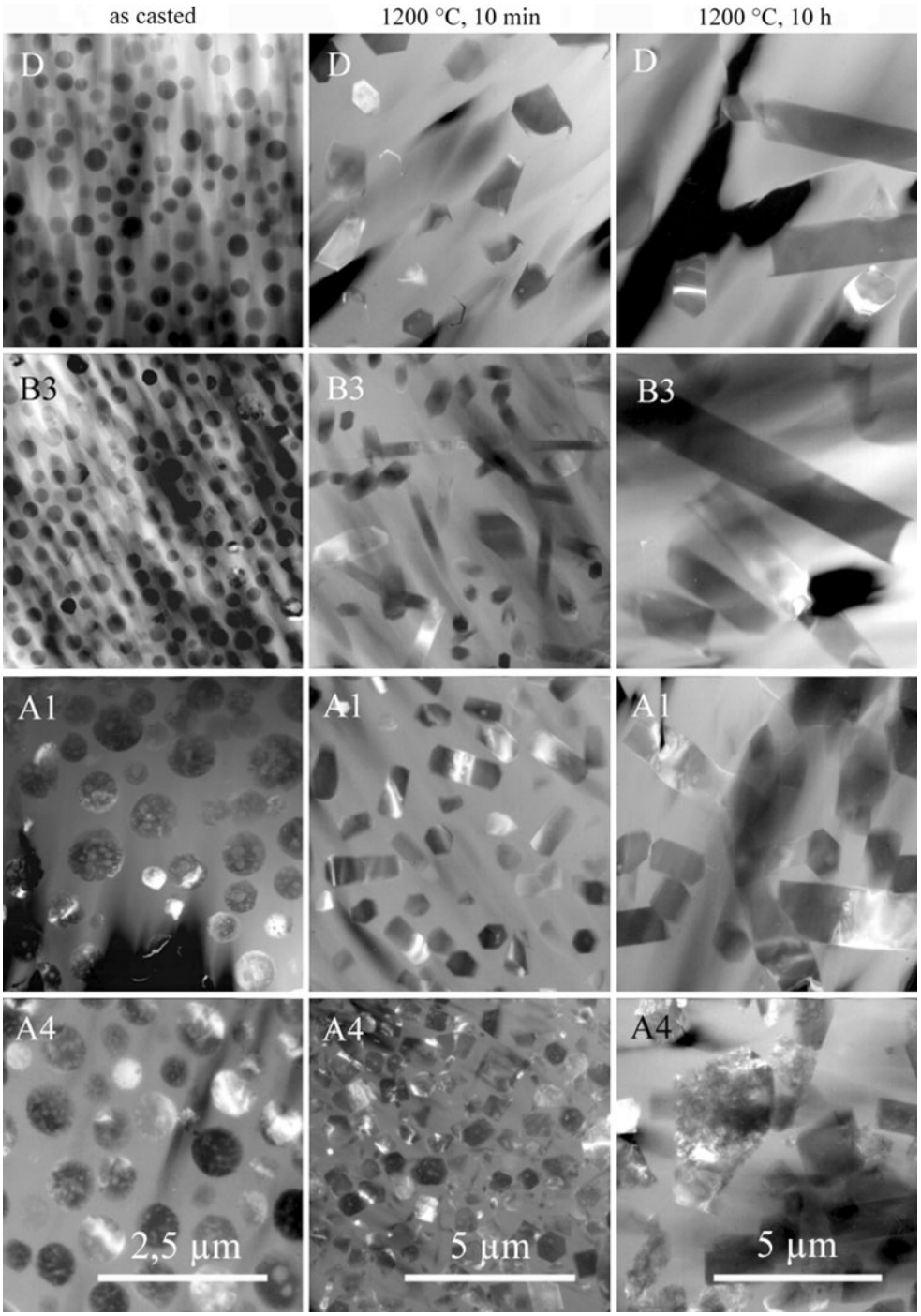


**Fig. 6** TEM bright-field and dark-field micrographs of glass with varying Ca/P ratio: D (Ca/P: 0.64, $29.8Al_2O_3{\cdot}19.8SiO_2{\cdot}25.2P_2O_5{\cdot}7.7K_2O{\cdot}9.2CaO{\cdot}8.4F^-$), B3 (Ca/P: 0.87, $25.5Al_2O_3{\cdot}18.6SiO_2{\cdot}27.3P_2O_5{\cdot}7.1K_2O{\cdot}13.6CaO{\cdot}8.0F^-$), A1 (Ca/P: 1.22, $0.5Na_2O{\cdot}23.5Al_2O_3{\cdot}17.1SiO_2{\cdot}26.6P_2O_5{\cdot}6.3K_2O{\cdot}18.6CaO{\cdot}7.4F^-$), A4 (Ca/P: 1.78, $0.2Na_2O{\cdot}23.0Al_2O_3{\cdot}15.6SiO_2{\cdot}24.1P_2O_5{\cdot}5.9K_2O{\cdot}24.6\ CaO{\cdot}6.7F^-$) after casting heat treatment for 10 min and 10 h at 1,200 °C (reproduced with copyright permission granted by Elsevier [28])

only recently, that a hypothesis was set out on the origin of the suppressed ripening in certain glass ceramics [37]. The idea is fairly simple but bears extensive consequences for the crystallization of glass in general: should the chemical composition of the precipitated phase not correspond to that of the residual glass (a non-isochemical system is dealt with), a highly viscous layer acting as a diffusion barrier can be formed around the growing crystals. Eventually, the

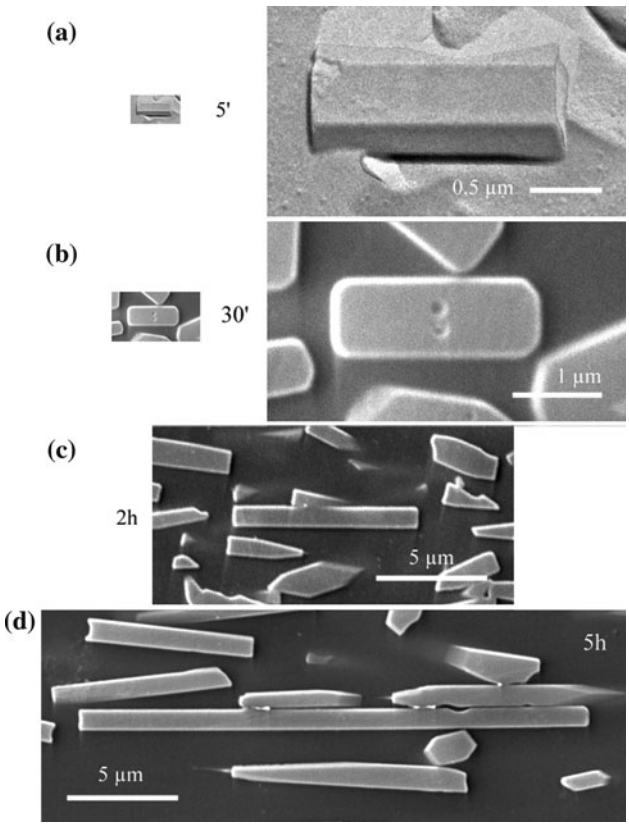


**Fig. 7** Electron micrographs of a $0.5Na_2O{\cdot}23.5Al_2O_3{\cdot}18.5SiO_2{\cdot}26.2P_2O_5{\cdot}6.8K_2O{\cdot}16.4CaO{\cdot}8.1F^-$ glass heat treated for 5 min (**a**, TEM replica film), 30 min (**b**), 2 h (**c**), and 5 h (**d**). Subfigures (**b**) to (**d**) are SEM secondary electron images. Left column of (**a**) and (**b**) are shown to scale with (**c**) and (**d**) (reproduced with copyright permission granted by ACS Publishing [30])

barrier can no longer become penetrated and the crystal growth comes to a stop.

In the case of lithia aluminosilicate glasses, however, things are even more complicated as shown in the following. In a model glass of the composition $3.5Li_2O{\cdot}0.15Na_2O{\cdot}0.2K_2O{\cdot}1.15MgO{\cdot}0.8BaO{\cdot}1.5ZnO{\cdot}20Al_2O_3{\cdot}67.2SiO_2{\cdot}2.6TiO_2{\cdot}1.7ZrO_2{\cdot}1.2As_2O_3$, titania and zirconia are added as nucleation agents, i.e. it is assumed that the latter two components would help promoting nucleation [38]. And in fact, as shown in Fig. 8, there is a multiplicity of tiny $ZrTiO_4$ precipitates that is extremely homogeneously distributed across the volume of the glass already after some very short heat treatment.

Now, as chemical composition enters the scene, another capability of transmission electron microscopy gets crucially important: nanoanalytics. Using the latter, beyond just imaging the chemical composition can be probed on the nanoscale. Here, novel technological developments accomplished within the past 10 years are of benefit as with the practical realization of aberration correction in electron optics extremely fine electron probes can be formed (down to less than 1 Å in diameter) even at reduced acceleration voltages (e.g. 80 keV). The latter aspect is of great relevance, as many glasses and glass ceramics can hardly be imaged or probed with electrons possessing energies in excess of 100 to 200 keV. Such technical preconditions given, an EELS line scan (like the 30 nm long one depicted in Fig. 8a) can be easily made and the ratio of elements can be determined for each data point. In the present case (Fig. 8b), it is found that the Al/Si ratio is significantly increasing when approaching the immediate interface between the residual glass and the $ZrTiO_4$ nanocrystal. In the glass under consideration here, the several nanometres large zirconiumtitanate nanocrystals, however, only act as nucleation agents. Contrary to the earlier hypothesis of epitaxial overgrowth (the latter has never been proved experimentally), another growth model literally obtrudes itself: in the evolving compositional gradient surrounding the $ZrTiO_4$ precipitate, there is (i) a wide choice of possible glass compositions to be used to commence nucleation of the secondary lithiumaluminosilicate crystal phase, (ii), due to these gradients, diffusion processes are likely to occur which can help further promoting the nucleus to grow.[1] It is currently not yet clear, but subject to ongoing investigations, whether or not the formation of liquid–liquid phase-separation droplets can also be accompanied by the formation of such diffusion barrier. Moreover, in other ongoing studies, nanoanalytics shall establish an experimental basis to decide whether the barrier is subjected to temporary changes upon heat treatment. Corresponding theoretical concepts and models need urgently to become elaborated [39–41] (Fig. 9).

## Aluminosilicate glass ceramics hosting $BaF_2$, $CaF_2$ or $LaF_3$

The precipitation of fluorides in glasses is appealing for applications in photonics as rare-earth doped $BaF_2$, $CaF_2$, as well as $LaF_3$ nanocrystals feature enhanced fluorescence [42, 43], luminescence [13, 44], optical amplification [42, 45], and up-conversion [46–48]. Oxyfluoride glasses combine the high transparency and durability of silicate glasses with the properties of fluoride phases that are known to have the capability to host rare-earth ions. Upon converting oxyfluoride glasses into fully transparent glass ceramics, following the conceptual ideas set out by Beall and Duke [10], optical properties become further enhanced. For photonic applications, size, size distribution and

[1] Similar arguments do apply to another unresolved issue of glass crystallisation, as it could be shown recently that there is the possibility of chemical "reconstruction" of surfaces leading to circumstances where surface crystallisation starts a few nanometres below the real surface [38].

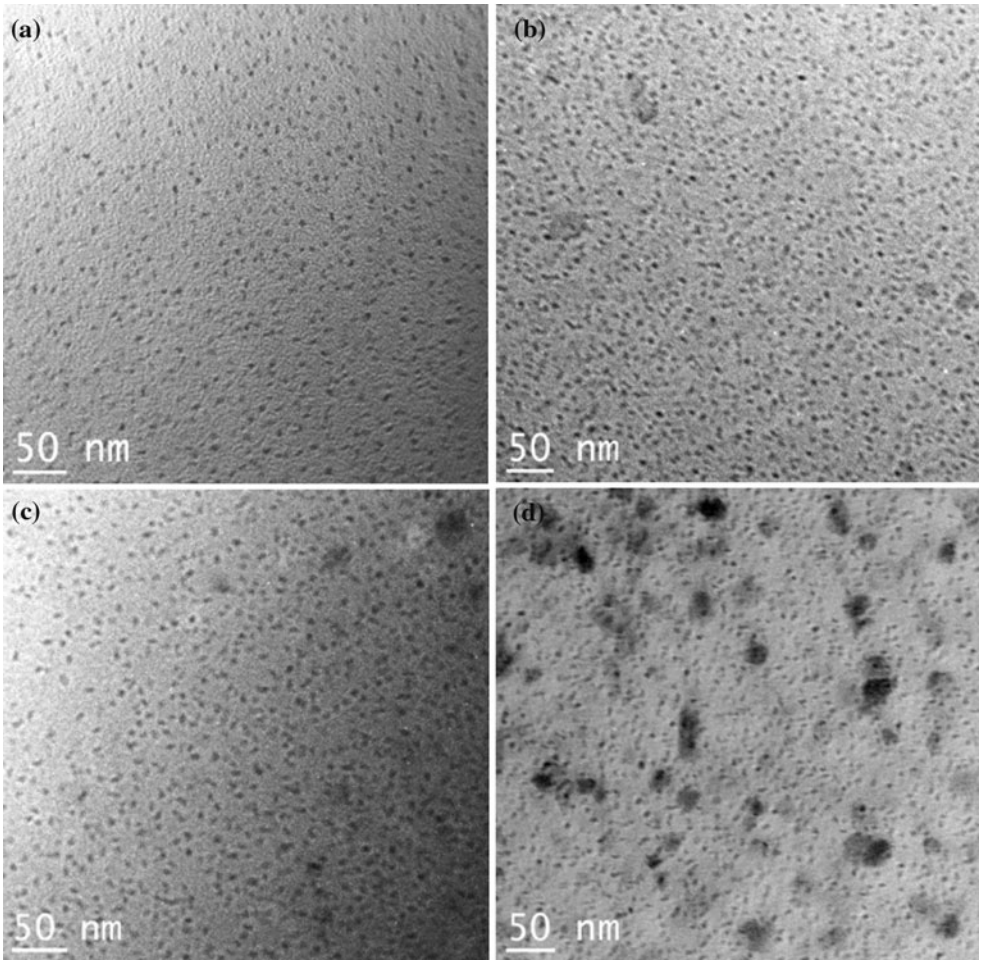


**Fig. 8** Bright-field TEM images (75 keV) of a $3.5Li_2O{\cdot}0.15Na_2O{\cdot}0.2K_2O{\cdot}1.15MgO{\cdot}0.8BaO{\cdot}1.5ZnO{\cdot}20Al_2O_3{\cdot}67.2SiO_2{\cdot}2.6TiO_2{\cdot}1.7ZrO_2{\cdot}1.2As_2O_3$ glass cerammed at 750 °C for **a** 1/2 h, **b** 1 h, **c** 2 h, and **d** 8 h (reproduced with copyright permission granted by ACS Publishing [38])

volume concentration of fluoride crystallites are decisive. In order to be suitable for optics, the size of the crystallites should be smaller than at least half of the wavelength of the light used while the size distribution should be as narrow as possible and the spatial distribution of crystallites ought to be very homogeneous. According to scattering theories by Rayleigh [49] and Mie [50], full transparency can be attained. In transparent oxyfluoride glass ceramics, the optically active (rare-earth) ion, e.g. $Er^{3+}$ or $Eu^{3+}$, tends to be located in the crystalline fluoride phase. As this results in significantly lower phonon energies, the intensity of the characteristic laser emission gets significantly increased while fluorescence lifetimes and up-conversion efficiencies become enhanced [51–53].

In view of the aforementioned self-limited growth imposed by the formation of a diffusion barrier, it seems challenging to scrutinize the presence of similar phenomena in fluoride-precipitating glasses as well. An in fact, the first experimental proof of the existence of such diffusion barrier was presented for the precipitation of $BaF_2$ from an aluminosilicate glass [54]. A first indication was found in energy-filtered (EF) TEM micrographs indicating an enrichment of silicon at the interface crystal-matrix. In EFTEM, electrons forming a magnified image of the electron-transparent sections of the sample are sent through an energy filter. Therefore, either only elastically scattered electrons (no energy loss, so-called zero-loss filtering) or electrons possessing characteristic losses evoked by element-specific absorption (by exciting ionisation of bound electrons into unoccupied higher states) can be selected [55].

It shall, however, not be concealed that EFTEM imaging can only be successfully applied if:

(i) the energy loss of the element in question is not too large (as a rule of thumb, well below 1 keV),
(ii) the element has a relative concentration above ca. 10 mol.%,

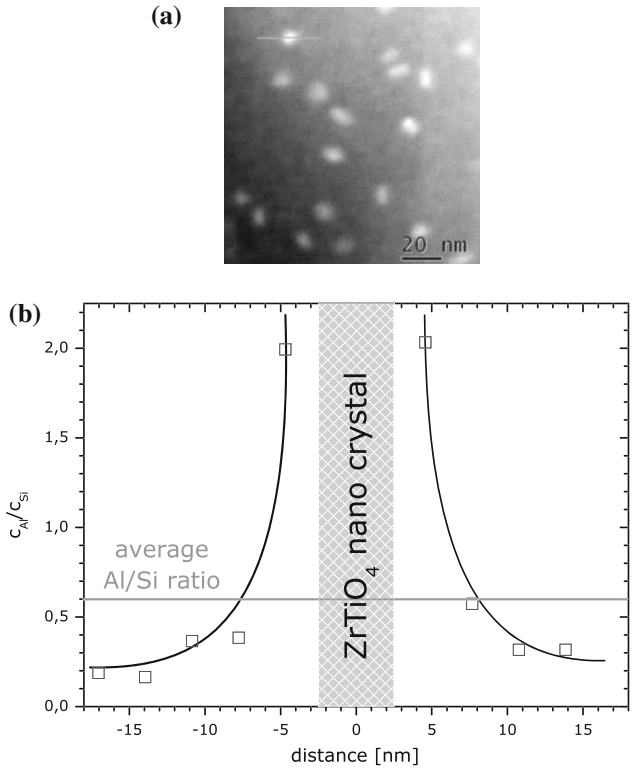


**Fig. 9** **a** Dark-field STEM micrograph (annual dark-field detector) of a $3.5Li_2O{\cdot}0.15Na_2O{\cdot}0.2K_2O{\cdot}1.15MgO{\cdot}0.8BaO{\cdot}1.5ZnO{\cdot}20Al_2O_3{\cdot}67.2SiO_2{\cdot}2.6TiO_2{\cdot}1.7ZrO_2{\cdot}1.2As_2O_3$ glass heat treated at 750 °C for 1 h with the location of line scan EELS analyses indicated across a crystal, **b** Al/Si ratio of along the line scan across the crystal shown in (**a**). *Solid lines* are guides to the eye to underline the resemblance with the simulated concentration profiles (reproduced with copyright permission granted by ACS Publising [38])

(iii) a spatial resolution below a few tenths of a nanometre is not aimed at (the actual resolution mainly depends in the amount of electron-optical aberrations, the acceleration voltage and the specific energy loss and is on the order of several nanometres),

(iv) there is no overlap of adjacent ionisation edges (the width of the energy window used to filter the required signal is usually chosen to be ca. 10 eV and as background subtraction is necessary to obtain decent results, also another few tens of electron volts below the edge onset interfering spectral features must not occur).

Some of those restrictions can be demonstrated for a $69.6SiO_2{\cdot}7.52Al_2O_3{\cdot}15.04K_2O{\cdot}1.88Na_2O{\cdot}6BaF_2$ glass [12, 54]. As shown in Fig. 10, the positions of nanocrystals (appearing dark in Fig. 10a) correspond to increased intensity in the EFTEM image shown in Fig. 10b. However, as illustrated by Fig. 11, there is a severe overlap of the Si-$L_{2,3}$ and the Ba-$N_{4,5}$ ionisation edge that cannot be separated with the settings used to obtain a reasonable

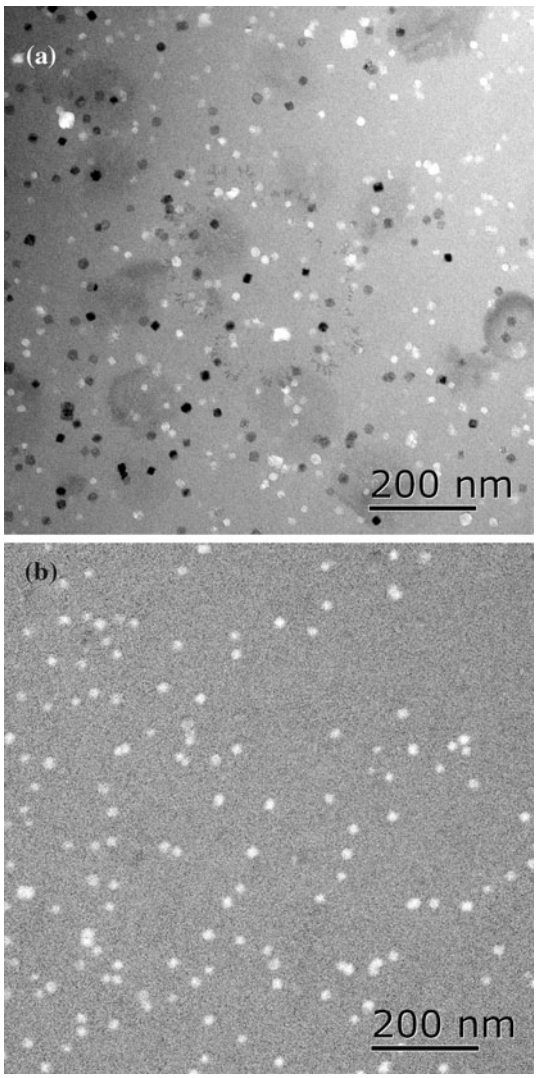


**Fig. 10** **a** Zero-loss filtered bright-field TEM image of a $69.6SiO_2{\cdot}7.52Al_2O_3{\cdot}15.04K_2O{\cdot}1.88Na_2O{\cdot}6BaF_2$ nanoglass ceramics, **b** Corresponding silicon map (reproduced with copyright permission granted by ACS Publising [54])

signal-to-noise ratio (energy window: 10 eV wide). A more detailed analysis revealed that the diameter of the bright spots visible in the EFTEM map is on average about 2 nm larger than the diameter of the nanocrystals imaged in the bright-field TEM micrograph. Taken together with EFTEM simulations [56] as well as spot analyses, the conclusion of a silicon enrichment at the periphery of the $BaF_2$ nanocrystals could be drawn though.

In the case just described, nanocrystals nucleate and subsequently grow within the residual glass matrix. However, in other glasses, such as the $40SiO_2{\cdot}30Al_2O_3{\cdot}18Na_2O{\cdot}12LaF_3$ glass shown prior to and after heat treatment in Fig. 12, phase-separation precedes the nucleation and crystallization [8, 9]. The answer to the question as to whether or not the size of phase-separation droplets may be

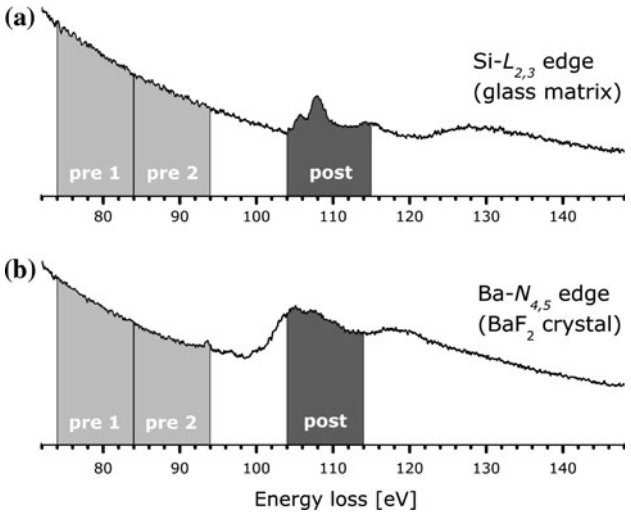


**Fig. 11** **a** Si-$L_{2,3}$ ELNES (residual $69.6SiO_2{\cdot}7.52Al_2O_3{\cdot}15.04K_2O{\cdot}1.88Na_2O{\cdot}6BaF_2$ glass), **b** Ba-$N_{4,5}$ ELNES acquired from a $BaF_2$ nanocrystal (reproduced with copyright permission granted by ACS Publising [54])

limited by a diffusion barrier (and not just determined by the cooling rate applied) is currently under intense study. However, with this example, another complication can be nicely illustrated. The composition of the liquid–liquid phase-separation droplets does not necessarily correspond to the composition of a crystalline phase that may become precipitated within the droplets. Such situation is exemplified in Fig. 13, where, along with a bright-field image, a Si elemental distribution map is shown. While lanthanum is already strongly enriched in the droplets (where upon annealing $LaF_3$ nanocrystals are formed), there is surplus silicon that gets pushed aside during crystallization.

## Electrochemically induced crystallization

Beyond in-depth analyses of the nucleation and crystallization phenomena discussed so far, direct control of nucleation and crystallization of glasses is the logical continuation. One such approach is based on the finding that polyvalent elements can change their role in a glass network from a network former into a network modifier [57–61].

As an example, fresnoitic glasses ($2BaO{\cdot}TiO_2{\cdot}2 + xSiO_2$) were supercooled in a crucible in which a platinum wire was introduced to act as a cathode [5]. When an electric current is allowed to flow through the melt, electrons emerging from the cathode do reduce the $Ti^{4+}$ towards $Ti^{3+}$ [62]. Such reduction is, in the case of titanium, accompanied with a switching from network forming to network modifying properties as the viscosity of the melt gets locally reduced. As a result, in the vicinity of the cathode, nucleation started and by growth selection, an oriented solidification of fresnoite ($Ba_2TiSi_2O_8$) commences. The preparation of such glass ceramics via controlled nucleation is practically important as fresnoite possesses very distinct piezoelectric properties, which require a high degree of texturing. In the case of fresnoite, single-crystal growth (by Czochralski pulling) [63] is possible, but similar to $Ba_2TiGe_2O_8$ [4, 64], $Ba_2TiSi_2O_8$ is highly brittle and applications (e.g. as hydrophone) [6, 7] often require mechanically rugged materials. With the addition of surplus silica, highly textures fresnoite crystals can become embedded into a matrix mainly consisting of silica glass. It was also reported that crystallization of fresnoitic glasses can be accomplished by internal irradiation with ultrashort laser pulses [65–67]. This effect is very

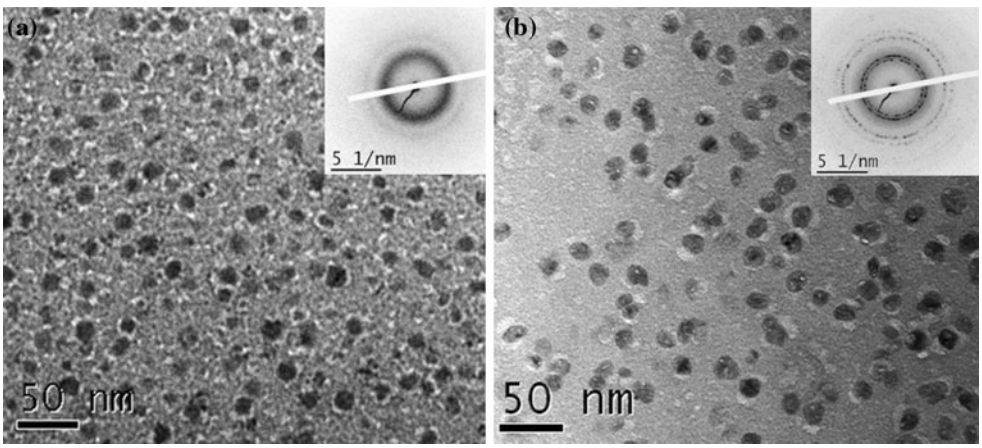


**Fig. 12** Zero-loss filtered bright-field TEM images (energy slit width: 10 eV) of: **a** the $40SiO_2{\cdot}30Al_2O_3{\cdot}18Na_2O{\cdot}12LaF_3$ glass, and **b** the $40SiO_2{\cdot}30Al_2O_3{\cdot}18Na_2O{\cdot}12LaF_3$ glass ceramics. *Insets* show respective selected-area electron diffraction patterns (reproduced with copyright permission granted by Elsevier [9])

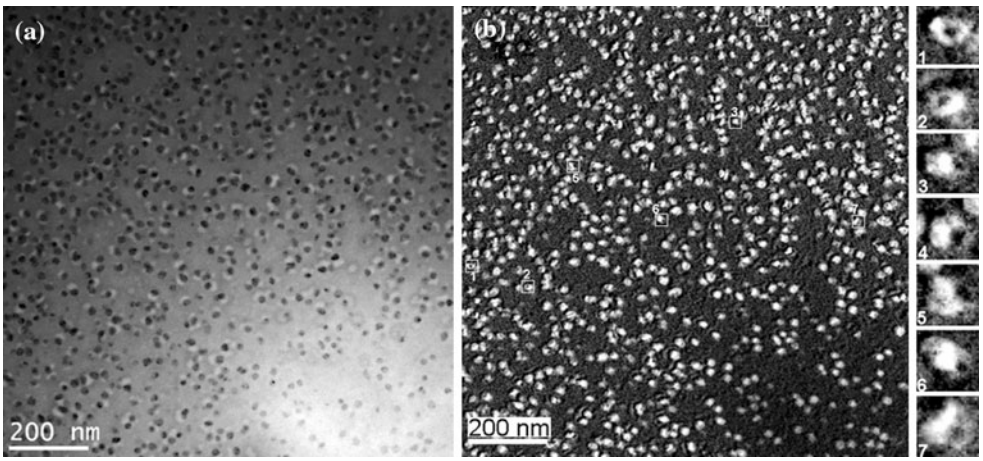


**Fig. 13** **a** Zero-loss filtered bright-field TEM image of the heat-treated $40SiO_2{\cdot}30Al_2O_3{\cdot}18Na_2O{\cdot}12LaF_3$ glass, and **b** corresponding Si-$L_{2,3}$ map. *Column to the right*: blow-ups of seven typical bright regions indicated by numbers in the image itself (reproduced with copyright permission granted by Elsevier [9])

likely to be related to a localized reduction of the glass, too, as femtosecond laser pulses have been shown by TEM/EELS to have a tremendous impact on the chemistry and network structure of glasses [68, 69].

## Limits of TEM characterization

In the examples discussed so far, a confinement was made to the discussion of particularly illustrative examples. Despite the fact that this might have been done on the expense of other, perhaps practically more important glass ceramics like the magnesium alumino silicate glass ceramics [70, 71], SiOC glasses [72], mullite-precipitating barium or boron alumino silicate glasses [11] etc., it is hoped that the great amount of diversity among nucleation and crystal growth phenomena in glasses could be demonstrated. In particular, it should be emphasized that the current understanding of nucleation and growth of nanocrystals is essentially based on often not applicable preconditions like the isochemical nature of base glass and crystalline precipitate. The importance of considering this fact could be proved by recent TEM experiments utilizing cutting-edge instrumentation.

Now, for the general case, the question might arise where the limits of TEM characterization (both with respect to imaging and the analytics) are reached. Therefore, in the following, a few major points shall be addressed.

### Minimum detectable size of nanocrystals

In transmission electron microscopy, there are generally two ways to image on the atomic scale: multi-beam interference in high-resolution TEM (HRTEM) or scanning TEM (STEM) using an extremely fine probe (nowadays down to a diameter of less than an Ångström. While HRTEM was demonstrated to work very well for the characterization of defects (such as grain boundaries, dislocation cores, etc.) in ceramics [73–75], there is a minimum size, a nanocrystal should possess to generate the required interference. Depending on the lattice-plane spacing (and therefore on the crystal structure of the precipitate), as a rule of thumb 5–7 lattice-plane spacings or roughly 2–3 nm holds [76]. With STEM, which resembles channelling contrast, smaller aggregates can be detected as recently show for a ca. 300 atom gold cluster [77]. While single lanthanum ions have been successfully localized in glassy films in contact to crystalline $Si_3N_4$ [78], for not as heavy elements the very early stages of nucleation can unfortunately not to spotted.

A further approach would include the study of electron energy-loss near-edge structures (ELNES) that reflect the first coordination sphere of the target ion and hence can be used beyond the capabilities of imaging techniques. It has been shown that ELNES spectroscopy can be readily applied to the study of valence [80] and coordination [79] of elements with suitable ionisation edges. Exemplified with fresnoitic glasses, it has not only been shown that ELNES spectroscopy can be applied to glasses [64, 80, 81], but its sensitivity is high enough to monitor structural discrepancies between casted glass and amorphized crystals of identical composition [82]. Here, the spatial resolution that can be attained with the finely probed beam is advantageous over related techniques like X-ray absorption near-edge structure spectroscopy (XANES) [83].

### Artefact-free samples as the ultimate limit

In order to max out the fabulous capabilities of transmission electron microscopy, extremely thin sections (just a

few tens of nanometres thick) of the glasses or glass ceramics under consideration need to be prepared without introducing artefacts. The common way to prepare electron-transparent sections is to mechanically pre-thin the material and remove the remaining 15 μm or so by ion-beam etching. Even if relatively low acceleration voltages (some 2.5 kV for $Ar^+$ ions) are used (and hence substantial warming of the sample is effectively suppressed) or even an ion polishing (at a few 100 eV acceleration voltage) is applied, the surface of the sample will always become amorphized to a depth of more than 1 nm. This effect can by no means be avoided (at least as long as ion beams are involved) but potentially distorts attainable results.

Moreover, charging of the often non-conducting materials must be avoided. In this respect, selective carbon coating proved very beneficial [84]. In this approach, electron-transparent parts of the sample are hidden behind an adapted mask during carbon coating. Such selective coating results, due to the pronounced surface diffusivity of carbon, in a conducting film behind the mask of ca. one-tenth of the original film thickness. During TEM imaging and analyses, the film is thick enough to drain the charge but thin enough to be not prone to contamination caused by the formation of carbon hillocks by surface diffusion. Another advantage is the larger C-film thickness at the periphery improving the electrical contact to the sample holder.

Another issue is radiation damage upon electron irradiation that ought to become reduced as much as possible. Possible mechanisms of radiation damage, ranging from viscous flow [85] over hole drilling to the accumulation of material within the irradiated area [86] are the subject of ongoing research. To this end, the availability of aberration-corrected electron microscopes that can be operated with high spatial resolution at reduced acceleration voltages of 80 or even 60 keV is largely advantageous. It does, however, increase the demands made to the quality of the samples as with reduced energy of the electrons, the samples gets virtually "thicker" (interaction cross-sections become larger, resulting in stronger scattering). In general, the usage of cooling holders proves advantageous for the reduction of damage to the specimen.

Last but not least, one might wonder whether or not in situ observation of crystallization processes would not be a great idea. However, attempts to follow up crystallization by in situ TEM are scarce [87, 88]. This is because environmental conditions are substantially different for the extremely thin sections being electron transparent: the surface–volume ratio is drastically changed towards a dominating surface, the irradiated parts reside in high or ultrahigh vacuum and manifold kinds of activation (see above) of the sample may be provoked by intense irradiation with electrons. Moreover, even if the available hot stages (allowing for applying temperatures of up to 1,000 °C) would reach the requested ceramming temperature, the actual temperature of the location of observation remains somewhat doubtful as heat conduction, radiation losses, etc. might cause deviations of the local temperature from the value measured at a remote position. For example, in a mica glass ceramics, where the formation of mica crystals is preceded by the formation of mullite–aluminium borate solid-solution crystals [89], the latter phase dissolved within 2 h in the hot-stage sample holder at 800 °C, even without electron irradiation during heat treatment. Vaporization of volatile elements such as boron or alkalis is likely to be responsible for this effect. Findings such as the one described above severely spoil the utilization of in situ techniques.

## Summary

In conclusion, three things should have become evident in this review.

(i) In glasses, an incredible variety of growth phenomena can possibly occur and it is essential to discriminate between isochemical and non-isochemical systems. In particular, our current understanding of the latter is incomplete and theoretical models need to be developed in the near future to be able and exploit the huge potential of crystalline phases precipitated in the latter glasses.

(ii) As the best basis of all theoretical treatment are systematic experiments, spatially and analytically highly resolved transmission electron microscopy is expected to play a major role in gaining a deeper understanding of nucleation and growth processes upon ceramming of glasses. It should, however, always kept in mind that in overstatement one might say that TEM is a matter of knowing everything about nothing, i.e. the information obtained is highly localized and generalization needs validation by integrating methods such as X-ray or neutron diffraction, multiquantum nuclear magnetic resonance spectroscopy, infrared spectroscopy, etc.

(iii) There is "electron amorphousness" (corresponding to X-ray amorphousness). This is, nanocrystals on the borderline to clusters, particularly, when embedded into an amorphous matrix cannot be directly imaged, nor can nuclei become visualized. To this end, there is hope that, at least for agglomerations of heavy elements, high-angle annular dark-field (HAADF) imaging might help imaging single atoms. Encouraging results were recently reported on the ordering of lanthanum ions in a glassy environment

in close contact to a $Si_3N_4$ single crystal [78]. Even 3D annular dark-field imaging of individual atoms by aberration-corrected STEM seems to be a viable option for the study of nucleation [90, 91].

Micro- and nanostructural investigations at glasses using TEM ever and ever again demonstrate the huge potential of this class of materials and the usefulness of TEM techniques for the characterization of the micro- and nanostructure. Depending on the composition and details of the heat treatment schedule, exciting phenomena show up in this realm of diversity.

**Acknowledgements** Fruitful discussions with and contributions of C. Rüssel, I. Avramov, R. Keding, S. Habelitz, C. Moisescu, A. Gebhardt, C. Bocker, R. Wurth, S. Bhattacharyya, J. Jinschek, as well as financial support by Deutsche Forschungsgemeinschaft (INK 6, HO/1691/5) and the European Commission (NMP3-CT-2006-033200) are gratefully acknowledged.

## References

1. Vogel W (1994) Glass chemistry. Springer, Berlin
2. Vogel W, Horn L, Reiss H, Völksch G (1982) J Non-Cryst Solids 49:221
3. Becker O, Bange K (1993) Ultramicroscopy 52:73
4. Höche T, Esmaeilzadeh S, Uecker R, Lidin S, Neumann W (2003) Acta Cryst B 59:209
5. Höche T, Keding R, Rüssel C, Hergt R (1999) J Mater Sci 34:195. doi:10.1023/A:1004423220508
6. Markgraf SA, Halliyal A, Bhalla AS, Newnham RE (1985) Ferroelectrics 62:17
7. Halliyal A, Bhalla AS, Markgraf SA, Cross LE, Newnham RE (1985) Ferroelectrics 62:27
8. Bhattacharyya S, Höche T, Hahn K, van Aken PA (2009) J Non-Cryst Solids 355:393
9. Bhattacharyya S, Höche T, Hémono N, Pascual MJ, Aken PAv (2009) J Cryst Growth 311:4350
10. Beall GH, Duke DA (1968) J Mater Sci 4:340. doi:10.1007/BF00550404
11. Beall GH, Pinckney LR (1999) J Am Ceram Soc 82:5
12. Bocker C, Bhattacharyya S, Höche T, Rüssel C (2009) Acta Mater 57:5956
13. Dejneka MJ (1998) J Non-Cryst Solids 239:149
14. Beall GH (1974) Mica glass-ceramics. US Patent 3,801,295
15. Grossmann DG (1972) J Am Ceram Soc 55:446
16. Vogel W, Höland W, Naumann K, Gummel J (1986) J Non-Cryst Solids 80:34
17. Quinn JB, Sundar V, Lloyd IK (2003) Dent Mater 19:603
18. Höland W, Wange P, Naumann K, Vogel J, Carl G, Jana C, Götz W (1991) J Non-Cryst Solids 129:152
19. Gebhardt A, Höche T, Carl G, Khodos II (1999) Acta Mater 47:4427
20. Höche T, Habelitz S, Avramov I (1999) Acta Mater 47:735
21. Habelitz S, Carl G, Rüssel C, Marchetti K, Röder E, Eifler D, Hergt R (1997) Glastechn Ber Glass Sci Technol 70:86
22. Höland W, Götz W, Carl G, Vogel W (1992) Cells Mater 2:105
23. Kokubo T, Shigematsu M, Hagashima Y, Tashiro T, Nakaura T, Yamamuro T, Higashi H (1982) Bull Inst Chem Red Kyoto Univ 30:260
24. Avery JK (1994) Oral development and histology. Thieme Medical Publishers, New York
25. Hill R, Wood D (1995) J Mater Sci Mater Med 6:311
26. Höland W, Frank M, Schweiger M, Rheinberger V (1994) Glastech Ber Glass Sci Technol 67C:117
27. Müller R, Abu-Hilal LA, Reinsch S, Höland W (1999) J Mater Sci 34:65. doi:10.1023/A:1004457305970
28. Moisescu C, Höche T, Carl G, Keding R, Rüssel C, Heerdegen WD (2001) J Non-Cryst Solids 289:123
29. Höche T, Moisescu C, Avramov I, Rüssel C, Heerdegen WD (2001) Chem Mater 13:1312
30. Höche T, Moisescu C, Avramov I, Rüssel C, Heerdegen WD, Jäger C (2001) Chem Mater 13:1320
31. Mary TA, Evans JSO, Vogt T, Sleight AW (1996) Science 272:90
32. Pryde AKA, Hammonds KD, Dove MT, Heine V, Gale JD, Warren MC (1996) J Phys Condens Matter 8:10973
33. Müller G, Hoffmann M, Neeff R (1988) J Mater Sci 23:1779. doi:10.1007/BF01115722
34. Pillars WW, Peacor DR (1973) Am Miner 58:681
35. Pannhorst W (1997) J Non-Cryst Solids 219:198
36. Henschel R, Höness H, Müller R, Reisert N (eds) (1995) Conventional production of Zerodur™. Springer, Berlin, Heidelberg, New York
37. Rüssel C (2005) Chemistry of materials 17:5843
38. Bhattacharyya S, Höche T, Jinschek JR, Avramov I, Wurth R, Müller M, Rüssel C (2010) Cryst Growth Des 10:379
39. Avramov I (2008) J Non-Cryst Solids 354:4959
40. Avramov I, Rüssel C, Kolkovska N, Georgiev I (2008) J Phys Condens Matter 20:335203
41. Tsakiris N, Argyrakis P, Avramov I, Bocker C, Rüssel C (2010) EPL 89:18004
42. Tanabe S, Hayashi H, Hanada T, Onodera N (2002) Opt Mater 19:343
43. Chen DQ, Wang YS, Yu YL, Ma E, Hu ZJ (2005) J Phys Condens Matter 17:6545
44. Yanes AC, Del-Castillo J, Mendez-Ramos J, Rodriguez VD, Torres ME, Arbiol J (2007) Opt Mater 29:999
45. Kawamoto Y, Kanno R, Qiu J (1998) J Mater Sci 33:63. doi:10.1023/A:1004333310532
46. Biswas A, Maciel GS, Kapoor R, Friend GS, Prasad PN (2003) J Non-Cryst Solids 316:393
47. Hu ZJ, Wang YS, Bao F, Luo WQ (2005) J Non-Cryst Solids 351:722
48. Patel DN, Reddy RB, Nash-Stevenson SK (1998) Appl Opt 37:7805
49. Strutt JW (3rd Baron Rayleigh) (1871) Philos Mag XLI:107
50. Mie G (1908) Ann Physik 330:377
51. Qiao X, Fan X, Wang M (2006) Scr Mater 55:211
52. Qiao X, Luo Q, Fan X, Wang M (2008) J Rare Earths 26:883
53. Dwivedia Y, Rai SB (2008) Opt Mater 31:87
54. Bhattacharyya S, Bocker C, Heil T, Jinschek JR, Höche T, Rüssel C, Kohl H (2009) Nano Lett 9:2493
55. Krivanek OL, Kundmann MK, Kimoto K (1995) J Microsc 180:277
56. Knippelmeyer R, Kohl H (1999) J Microsc 194:30
57. Avramov I, Keding R, Rüssel C (2000) Glass Sci Technol Glastech Ber 73:138
58. Avramov I, Keding R, Rüssel C (2000) J Non-Cryst Solids 272:147
59. Avramov I, Keding R, Russel C, Kranold R (2000) J Non-Cryst Solids 278:13
60. Avramov I, Rüssel C, Keding R (2003) J Non-Cryst Solids 324:29
61. Keding R, Avramov I, Rüssel C (2000) Glass Sci Technol Glastech Ber 73:338
62. Höche T, Kleebe H-J, Brydson R (2001) Philos Mag A 81:825

63. van Aken PA, Höche T, Heyroth F, Keding R, Uecker R (2004) Phys Chem Miner 31:543
64. Höche T, van Aken PA, Grodzicki M, Heyroth F, Keding R, Uecker R (2004) Philos Mag 84:3117
65. Honma T, Benino Y, Fujiwara T, Komatsu T (2006) Appl Phys Lett 88
66. Dai Y, Zhu B, Qiu JR, Ma HL, Lu B, Cao SX, Yu BK (2007) Appl Phys Lett 90
67. Zhu B, Dai Y, Ma HL, Zhang SM, Lin G, Qiu JR (2007) Opt Express 15:6069
68. Su D, Jiang N, Qiu JR, Spence JCH (2009) J Mater Res 24:1983
69. Zhou SF, Lei WQ, Jiang N, Hao JH, Wu E, Zeng HP, Qiu JR (2009) J Mater Chem 19:4603
70. Carl G, Höche T, Voigt B (2002) Phys Chem Glasses 43C:231105
71. Wange P, Höche T, Rüssel C, Schnapp ED (2002) J Non-Cryst Solids 298:181109
72. Gregori G, Kleebe HJ, Readey DW, Soraru GD (2006) J Am Ceram Soc 89:1699
73. Höche T, Kenway PR, Kleebe H-J, Finnis MW, Rühle M (1994) J Phys Chem Solids 55:1067
74. Höche T, Kenway PR, Kleebe H-J, Rühle M (1994) J Am Ceram Soc 77:339
75. Höche T, Rühle M (1996) J Am Ceram Soc 79:1961
76. Höche T, Angermann T (2000) J Non-Cryst Solids 262:114
77. Li ZY, Young NP, Di Vece M, Palomba S, Palmer RE, Bleloch AL, Curley BC, Johnston RL, Jiang J, Yuan J (2008) Nature 451:46-U42
78. Shibata N, Pennycook SJ, Gosnell TR, Painter GS, Shelton WA, Becher PF (2004) Nature 428:730
79. Höche T, Olhe P, Keding R, Rüssel C, Aken PAv, Schneider R, Kleebe H-J, Wang X, Jacobson AJ, Stemmer S (2003) Philos Mag 83:165
80. Höche T, Grodzicki M, Heyroth F, Aken PAv (2005) Phys Rev B 72:205111
81. Höche T, Heyroth F, Grodzicki M, Aken PAv (2005) Phys Stat Solid A 202:2355
82. Höche T, Schrempel F, Grodzicki M, Aken PAv, Heyroth F (2006) Chem Mater 18:46
83. Avramov I, Höche T, Henderson GS (2008) J Non-Cryst Solids 354:4681
84. Höche T, Gerlach JW, Petsch T (2006) Ultramicroscopy 106:981
85. Möbus G, Ojovan M, Cook S, Tsai J, Yang G (2010) J Nucl Mater 396:264
86. Egerton RF, Wang F, Crozier PA (2006) Microsc Microanal 12:65
87. Mallamaci MP, Bentley J, Carter CB (1994) In: Libera M, Haynes TE, Cebe P, Dickinson JE (eds) Crystallization and related phenomena in amorphous materials. Materials Research Society, Pittsburgh
88. Mallamaci MP, Bentley J, Carter CB (1997) Acta Mater 46:283
89. Habelitz S, Höche T, Hergt R, Carl G, Rüssel C (1999) Acta Mater 47:2831
90. van Benthem K, Lupini AR, Oxley MP, Findlay SD, Allen LJ, Pennycook SJ (2006) Ultramicroscopy 106:1062
91. van Benthem K, Lupini AR, Kim M, Baik HS, Doh S, Lee JH, Oxley MP, Findlay SD, Allen LJ, Luck JT, Pennycook SJ (2005) Appl Phys Lett 87:034104